aerospace

MDPI

Article

Optimization Design of Honeycomb Absorbing Structure and Its Application in Aircraft Inlet Stealth

Huimin Xiang [1], Yongqiang Shi [1,*], Qingzhen Yang [1], Xufei Wang [1] and Yubo He [2]

[1] School of Power and Energy, Northwestern Polytechnical University, Xi'an 710129, China; hmxiang@mail.nwpu.edu.cn (H.X.)
[2] Aerospace Era Feihong Technology Limited Company, Beijing 100080, China
* Correspondence: yqshi@nwpu.edu.cn

Abstract: The growing demand for stealth technology in military and aerospace applications has driven the development of advanced radar-absorbing structures. In particular, honeycomb absorbing structures (HASs) have shown promise due to their unique properties. In order to enhance the absorption characteristics of HASs and evaluate its application effect on aircraft, firstly, the mechanism of enhancing the electromagnetic (EM) absorption capacity of honeycomb structures by using a gradient design for the impregnation material is studied. Secondly, a multi-layer gradient honeycomb absorbing structure (MGHAS) with top skin and intermediate bonding layers is proposed. The influence of the type and arrangement of impregnation materials on reflectivity is analyzed to obtain design strategies that can enhance the absorption performance of the MGHAS. An improved particle swarm optimization (PSO) algorithm is proposed to optimize the EM absorption performance of the MGHAS. The optimized MGHAS achieves broadband absorption below −10 dB in a 2–18 GHz range, and the reflectivity even reaches −30 dB near 10 GHz. Finally, to solve the problem of electromagnetic scattering characteristics of periodic structures, such as HASs applied to electrically large targets, reflectivity is introduced into a shooting and bouncing ray method, which is a high-frequency algorithm used to analyze the electromagnetic scattering characteristics of the aircraft inlet. Based on this method, the reduction effect of the MGHAS on the radar cross section (RCS) of the aircraft inlet is explored. The results indicate that at the detection angle at 0° and detection frequency at 10 GHz, an aircraft inlet equipped with the MGHAS achieves a 26 dB reduction in the RCS compared with an aircraft inlet without stealth technologies and an 18 dB reduction compared with an inlet with coating-type absorbing material in TM mode. This study demonstrates that the proposed MGHAS effectively reduces the electromagnetic scattering intensity of the aircraft inlet and enhances the radar stealth performance of the aircraft.

Keywords: honeycomb absorbing structure; homogenization method; reflectivity; shooting and bouncing ray method; radar cross section (RCS); radar stealth

check for updates

Citation: Xiang, H.; Shi, Y.; Yang, Q.; Wang, X.; He, Y. Optimization Design of Honeycomb Absorbing Structure and Its Application in Aircraft Inlet Stealth. *Aerospace* **2024**, *11*, 796. https://doi.org/10.3390/aerospace11100796

Academic Editor: Sebastian Heimbs

Received: 12 August 2024
Revised: 12 September 2024
Accepted: 20 September 2024
Published: 27 September 2024

Copyright: © 2024 by the authors. Licensee MDPI, Basel, Switzerland. This article is an open access article distributed under the terms and conditions of the Creative Commons Attribution (CC BY) license (https://creativecommons.org/licenses/by/4.0/).

1. Introduction

With the rapid development of radar detection technology, aircraft stealth technology is also constantly developing. Since the main threat to aircraft originates from radar, and according to the current statistical analyses [1], radar poses a threat to aircraft, accounting for over 60%, the radar stealth capability of aircraft puts forward higher requirements.

Using radar-absorbing materials (RAMs) is an effective method to reduce the intensity of target radar echoes. It absorbs incident electromagnetic (EM) waves and converts them into other forms of energy, such as thermal energy inside the material [2]. Usually, RAMs can generally be divided into surface-coating materials and structural absorbing materials. Structural absorbing materials have both radar-absorbing and mechanical properties, which have been applied to stealth aircraft. Salisbury, Jaumann, Dallenbach, and honeycomb absorbing structures (HASs) are popular structural RAMs [3,4]. Among them, HASs mimic

the hexagonal honeycomb of a natural honeycomb and is a typical three-dimensional periodic structural absorbing material [5,6] which has the advantages of a wide-absorbing frequency bandwidth and high stiffness-to-weight ratios [7,8]; thereby, it can serve as a load-bearing component.

Although HASs have been successfully applied on many occasions, due to their thin-walled and multi-layer structure, the calculation of their scattering characteristics remains a huge challenge. The methods for studying their electromagnetic scattering characteristics mainly include experimental testing, direct numerical simulation, and homogenization methods. Direct numerical simulation requires the complete mesh discretization of the structure and periodic boundary conditions (PBCs) [9] and then the use of full wave methods such as finite difference time domain (FDTD) [10], the method of moments (MOM) [11], and the finite element method (FEM) [12,13]. These calculation results are more accurate but time-consuming. Especially in cases where optimization design requires a large number of sample calculations, the drawbacks of numerical methods being computationally expensive and time-consuming are even more evident.

However, homogenization methods have higher computational efficiency and are suitable for solving problems with structures when the geometric period is small compared with the wavelength [14]. Johansson [15] used Hashin–Shtrikman (HS) variational theory to derive a theoretical expression for obtaining the equivalent electromagnetic parameters (EEPs) of periodic structures and applied it to other structures, such as honeycombs and wedges. The calculation results were compared with the FEM to verify the feasibility and accuracy of the method. Quail et al. [16]. proposed a new EEP extraction method based on the partition domain method, which decomposes the basic units of periodic materials into fictitious vertical layers. Finally, the results were also compared with the FEM. On the basis of Quail's work, Chen [17] further derived the partition domain method applicable to normal honeycomb absorbing structures (NHASs). It was found that the electromagnetic parameter difference of HASs in the direction parallel to the honeycomb surface was very small, so they can generally be regarded as uniaxial anisotropic materials. Zhao [18] extracted the EEPs of HASs by using effective medium theory (EMT) [19,20], strong fluctuation theory (SFT) [21–23], and HS variational theory and compared the characteristics and applicability of different algorithms. He discovered that the reflectivity curve trends and absorption peaks obtained with different theories were basically consistent. He [24] found that the EEPs of HASs were all smaller than the electromagnetic parameters of impregnated materials. On the other hand, the decrease in the effective permittivity was greater than the permeability, a feature more conducive to satisfying the impedance matching of absorbing materials. It was also found that different honeycomb heights correspond to an optimal coating thickness, so it was necessary to reasonably design its structural parameters. Further, Zhao [25] designed a new HAS with a gradient change in the thickness of the coating material and obtained its physical structure through 3D-printing technology. The results showed that at a certain oblique angle, the reflectivity of the HAS was less than −10 dB in the angle range of 0°~70°, indicating that the gradient honeycomb absorbing structures (GHASs) had good microwave-absorbing properties. Zhou [26] and Zhao [27] studied the design, manufacturing, and analysis methods of GHASs and confirmed that the research method of equating them to multi-layer uniformly distributed structures is certainly reliable.

In addition, the design and optimization of HASs can further improve their absorbing performance within limits. Many relevant research studies have been conducted. Khurram [28] used experimental design methods to compare the absorbing characteristics of HASs with different thicknesses, carbon powder absorbing coatings, and skins in the frequency range of 2–18 GHz. The results indicated that there is an optimal coating weight ratio for HASs with different thicknesses, which maximizes the absorption bandwidth. He [29] explored a multi-section step-impedance honeycomb structure, which achieves impedance matching with free space and low-reflectivity requirements. The equivalent parameters were obtained by using the EMT method and transmission line theory [30],

and the particle swarm optimization (PSO) algorithm was used to obtain the optimal combination of multi-layer honeycomb height and absorbing coating materials. Zhao [27,31] analyzed the influence of the design parameters of GHASs on reflectivity, and optimized the absorption characteristics, again verifying the superiority of GHASs. Li [32] also proposed a multi-layer HAS and used the JAYA algorithm for multi-objective optimization research on the absorbing performance and load-bearing performance of the structure. Specifically, the absorbing bandwidth was used as an indicator to characterize the absorbing performance of the structure. The wave absorption performance of the optimized structure increased by 7.5%, and the optimized load-bearing performance increased by 167.4%. Sun [33] used the FDTD method to calculate the reflectivity of a double-layer HAS and used the orthogonal experimental design method to study HASs with different thicknesses and material combinations. It was found that the absorbing effect is related to the material combinations and thickness distribution of each layer. Zhang [34] also investigated the optimal design and analysis methods of multi-layer absorbing honeycomb composite structures.

Although progress has been made in the research of HASs, deficiencies still exist, particularly a lack of related research on the optimization of multi-layer structures and the application method of periodic structures to electrically large targets. In this paper, the homogenization method was applied to evaluate the electromagnetic wave absorption performance of normal and gradient honeycomb absorbing structures at different bandwidths and angles, and the mechanism by which gradient impregnation enhances absorption performance was investigated. Then, a multi-layer gradient honeycomb absorbing structure (MGHAS) with top skin and intermediate bonding layers was developed. And the improved particle swarm optimization (PSO) algorithm was applied to optimize the EM absorption performance of the MGHAS. Finally, reflectivity was introduced into the high-frequency calculation method to analyze the electromagnetic scattering characteristics of an aircraft inlet equipped with the MGHAS and evaluate its performance in reducing radar cross section (RCS). This research can contribute to the advancement of stealth material technology and enhance the practical application of advanced materials in reducing the detectability of aircraft.

2. Theoretical Calculation Model and Methods

2.1. Theoretical Model

The HASs studied in this paper are shown in Figure 1. The single-layer structure has three parts, including a top skin, a middle honeycomb core absorbing layer and a bottom reflective layer. The top skin is made of glass fiber reinforced polymer (GFRP) material, while the central honeycomb core includes a honeycomb framework and a coating medium. The framework material is aramid paper. Unlike the single-layer structure, the multi-layer structure incorporates bonding layers to connect the honeycomb core absorbing layers, using epoxy as the bonding material. For clarity in subsequent descriptions, the honeycomb core adjacent to the reflective layer is designated as the first layer. This layer features a periodic ortho-hexagonal structure with the unit cell as its fundamental unit. The side length of the honeycomb framework is r, the thickness is w, and the height is h. In the configuration termed GHAS, the coating medium's thickness varies along the height, with the top and bottom thicknesses denoted by d_{top} and d_{bottom}, respectively. When the impregnation material maintains a constant thickness throughout its height, $d_{top} = d_{bottom}$.

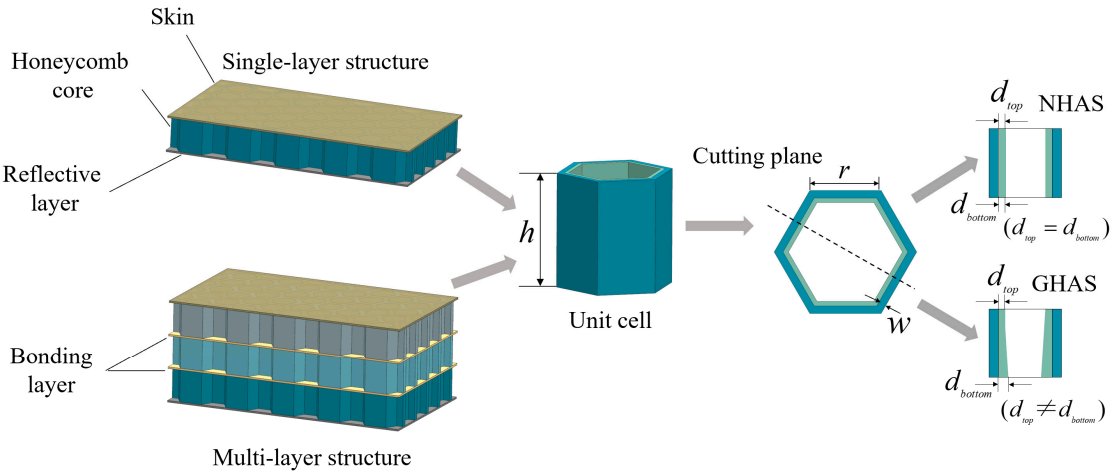

Figure 1. Schematic diagram of single-layer and multi-layer honeycomb structure with their compositions.

The detailed electromagnetic parameters for each component are listed in Table 1 [35,36]. The impregnation materials featured in Table 1 predominantly consist of Carbon Black, Iron/Nickel Oxide, and Epoxy Resin, with the addition of Mineral Oil and Polyethylene Glycol serving as dispersants and lubricants. By adjusting the mass percentage of these materials, the electromagnetic characteristics of the impregnation material can be finely tuned. It is important to note that the electromagnetic parameters of all materials discussed in this study are expressed as relative values.

Table 1. Electromagnetic properties of materials.

Material		ε_r'	ε_r''	μ_r'	μ_r''
Honeycomb Framework		2.4	0	1	0
Coating medium	RAM1	22.68	6.58	2.23	1.94
	RAM2	11.46	1.5	1.12	0.17
	RAM3	20.18	18.25	3.1	2.79
Skin		4.2	0.3	1	0
Bonding layer		2.9	0.008	1	0

2.2. Equivalent Electromagnetic Properties of Honeycomb Cores

Currently, the commonly used theories for extracting the equivalent electromagnetic parameters of honeycomb cores are EMT, HS variation theory, SFT, etc. Among them, HS starts from the microstructure of composite materials, adopts multi-scale technology and averaging progressive analysis technology, and can extract the EEPs from materials with periodic structures. This paper uses this method to extract the EEPs of HASs.

For the honeycomb structure in Figure 1, the electromagnetic parameters of the framework and the coating material are assumed to be $\varepsilon_{framework}$ and ε_{coat}, respectively. The corresponding duty cycles are assumed to be $\nu_{framework}$ and ν_{coat} respectively. According to HS theory [37], the upper and lower bounds are given below (assuming $\varepsilon_{framework} > \varepsilon_{coat}$).

Upper bound model:

$$\varepsilon_{eff,x,y} = \varepsilon_{framework} \frac{(1+\nu_{coat})\varepsilon_{coat} + (1-\nu_{coat})\varepsilon_{framework}}{(1-\nu_{coat})\varepsilon_{coat} + (1+\nu_{coat})\varepsilon_{framework}} \quad (1)$$

$$\varepsilon_{eff,z} = \nu_{framework}\varepsilon_{framework} + \nu_{coat}\varepsilon_{coat} \quad (2)$$

Lower bound model:

$$\varepsilon_{eff,x,y} = \varepsilon_{coat}\frac{(1+\nu_{framework})\varepsilon_{framework} + (1-\nu_{framework})\varepsilon_{coat}}{(1-\nu_{framework})\varepsilon_{framework} + (1+\nu_{framework})\varepsilon_{coat}} \tag{3}$$

$$\varepsilon_{eff,z} = \nu_{framework}\varepsilon_{framework} + \nu_{coat}\varepsilon_{coat} \tag{4}$$

In the above equation, the subscripts x, y, and z denote the equivalent parameters in the x, y, and z directions, respectively. Given that both the framework and the coating materials are generally isotropic media, there is no directional differentiation. It is established that the electromagnetic parameters of honeycomb structures exhibit slight variations in the direction parallel to the honeycomb surface; hence, they can be treated as uniaxial anisotropic materials. In the model discussed in this paper, the x- and y- axes lie on a plane parallel to the surface of the reflective layer; thus, $\varepsilon_{eff,x} = \varepsilon_{eff,y}$. When the modulus of $\varepsilon_{framework}$ exceeds ε_{coat}, an upper bound model is applied. Otherwise, a lower bound model is adopted. The method for calculating the equivalent permeability aligns with that for effective permittivity; simply replace $\varepsilon_{eff,x,y}$, $\varepsilon_{eff,z}$, $\varepsilon_{framework}$, and ε_{coat} with $\mu_{eff,x,y}$, $\mu_{eff,z}$, $\mu_{framework}$ and μ_{coat}, respectively.

2.3. Reflectivity of Multi-Layer Structure

Reflectivity is a crucial metric that effectively illustrates the electromagnetic performance of absorbing materials. In this study, it is employed to assess the electromagnetic absorption characteristics of HASs. Upon determining the EEPs of the honeycomb core structure, an HAS can be considered a uniaxial anisotropic multi-layer structure. Figure 2 illustrates an n-layer structure featuring a metal substrate as the reflective layer. In this figure, ε_i, μ_i, and d_i represent the complex permittivity, complex permeability, and thickness of the i-th layer, respectively. The top of the structure interfaces with free space. The angle θ denotes the direction of EM wave incidence, and z indicates the principal axial direction.

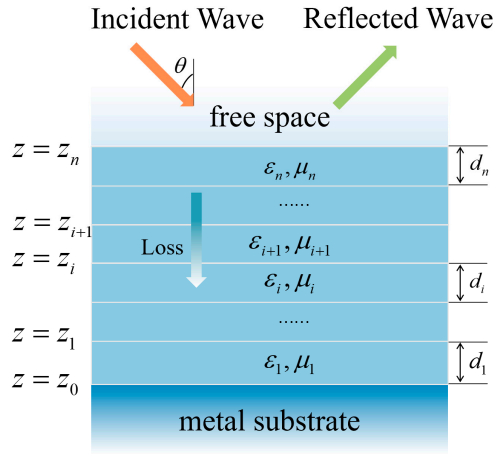

Figure 2. Illustration of electromagnetic wave propagation in multi-layered media with metal substrate.

Given that the traditional transmission line method is limited to isotropic materials, this study derives a new formula for calculating reflectivity, tailored specifically to multi-layer anisotropic materials, based on the principles of electromagnetic field theory.

In the propagation of EM waves through a multi-layer media structure, it is essential that these waves comply with the propagation laws within each medium and satisfy the boundary conditions at every interface. The detailed derivation presented in reference [38] addresses the scenario of oblique incident waves. Taking the transverse electric (TE) polarization mode as an example, the analysis commences at the interface between the i-th layer and the $(i + 1)$-th layer.

Assuming that E_i^+ and E_i^- are the amplitudes of the forward and reverse electric fields of the i-th layer respectively, the electric and magnetic fields of the i-th layer are given below.

$$\mathbf{E}_i = (E_i^+ g_i + E_i^- h_i)\mathbf{e}_y \tag{5}$$

$$\mathbf{H}_i = \frac{k_{z1,i}}{\omega\mu_0\mu_{xoy,i}}(-E_i^+ g_i + E_i^- h_i)\mathbf{e}_x + \frac{\sin\theta}{\eta_0\mu_{z,i}}(E_i^+ g_i + E_i^- h_i)\mathbf{e}_z \tag{6}$$

where

$$g_i = e^{-jk_o[x\sin\theta - jk_{z1,i}(z+z_{i-1})]} \tag{7}$$

$$h_i = e^{-jk_0[x\sin\theta + jk_{z1,i}(z+z_{i-1})]} \tag{8}$$

Similarly, by replacing i with i +1 in the previous equations, we obtain the expressions for the electric and magnetic fields in the (i + 1)-th layer. According to the boundary condition of tangential continuity for the electric and magnetic fields at the interface, we can obtain the equations below.

$$E_{i+1}^+ + E_{i+1}^- = E_i^+ e^{jk_{z1,i}d_i} + E_i^- e^{-jk_{z1,i}d_i} \tag{9}$$

$$\frac{k_{z1,i+1}}{\omega\mu_0\mu_{xoy,i+1}}(-E_{i+1}^+ + E_{i+1}^-) = \frac{k_{z1,i}}{\omega\mu_0\mu_{xoy,i}}(-E_i^+ e^{jk_{z1,i}d_i} + E_i^- e^{-jk_{z1,i}d_i}) \tag{10}$$

Reflectivity is defined in Equation (11).

$$\Gamma_{\mathrm{TE},i} = \frac{E_{i+1}^-}{E_{i+1}^+} \tag{11}$$

Putting Equations (9) and (10) into (11), we can obtain Equation (12).

$$\Gamma_{\mathrm{TE},i} = \frac{(m_{i+1} - m_i)e^{j2k_{z1,i}d_i} + (m_{i+1} + m_i)\Gamma_{\mathrm{TE},i-1}}{(m_{i+1} + m_i)e^{j2k_{z1,i}d_i} + (m_{i+1} - m_i)\Gamma_{\mathrm{TE},i-1}} \tag{12}$$

where

$$m_i = \sqrt{\frac{\varepsilon_{xoy,i}}{\mu_{xoy,i}} - \frac{\sin^2\theta}{\mu_{xoy,i}\mu_{z,i}}} \tag{13}$$

$$k_{z1,i} = k_0\sqrt{\varepsilon_{xoy,i}\mu_{xoy,i} - \frac{\mu_{xoy,i}}{\mu_{z,i}}\sin^2\theta} \tag{14}$$

Consider the initial value $\Gamma_{\mathrm{TE},0}$ of the recursive equation. Given that the tangential electric field on the surface of the metal substrate is zero, we set this condition when $z = 0$:

$$E_i^+ e^{-jk_{z1,1}x\sin\theta} + E_i^- e^{-jk_{z1,1}x\sin\theta} = 0 \tag{15}$$

We obtain the reflectivity from the first layer to the metal substrate in Equation (16).

$$\Gamma_{\mathrm{TE},0} = \frac{E_1^-}{E_1^+} = -1 \tag{16}$$

To summarize, when an EM wave is incident at an angle θ on an n-layer anisotropic medium with a metallic reflective substrate under the TE model, reflectivity can be calculated by using Equation (17).

$$\Gamma_{\mathrm{TE},i} = \begin{cases} -1\ (i = 0) \\ \frac{(m_{i+1} - m_i)e^{j2k_{z1,i}d_i} + (m_{i+1} + m_i)\Gamma_{\mathrm{TE},i-1}}{(m_{i+1} + m_i)e^{j2k_{z1,i}d_i} + (m_{i+1} - m_i)\Gamma_{\mathrm{TE},i-1}}\ (i = 1, 2, \ldots n) \end{cases} \tag{17}$$

The transverse magnetic (TM) polarization model is analogous to the TE model; therefore, it will not be detailed further here.

For convenience of expression, reflectivity is further formulated as presented in Equation (18).

$$RL = 20 \times \log(\Gamma) \tag{18}$$

2.4. Verification of Proposed Method

To verify the accuracy of the calculation method employed in this study, a GHAS is chosen as a representative example. Its reflectivity is determined by using the prescribed method, and the results are subsequently compared with those derived from the FEM in HFSS commercial software. To simulate the wave-absorbing characteristics of the GHAS, we use tetrahedral grids, periodic boundary conditions, and Floquet port excitation.

The specific parameters of the validation model are detailed in Table 2, and the materials correspond consistently to those listed in Table 1. For the calculation of the electromagnetic characteristics of the GHAS, we divide it into n layers evenly, ensuring that ν_{coat} and $\nu_{framework}$ remain unchanged in each layer. Each layer is then considered equivalent to an HAS with uniform coating thickness, as referenced in [26,27].

Table 2. Geometry and material parameters of validation model.

	h	d_{top}	d_{bottom}	r	w	*Material*
Honeycomb core	10	0.4	0.8	2	0.2	Honeycomb framework + RAM2
Skin	1	—	—	—	—	Skin medium

Figure 3 compares the calculation results obtained by using the HS method, as described in this paper, with those obtained with the FEM across various incident angles. The error is defined as the absolute value of the discrepancy between the two calculation methods. When the incident EM waves are at 0° and 30°, the reflectivity curves generated by the HS method and the FEM display a high degree of concordance, featuring similar change patterns and consistent positions of absorption peaks, particularly in the low frequency band. Only at the positions of several absorption peaks do the values obtained by the two methods display small deviations, which remain within an acceptable range. We observe that the resonance frequency intervals depicted in the figure exhibit a certain regularity, typically associated with the relationship between the geometric dimensions of the honeycomb structure and the incident EM wavelength.

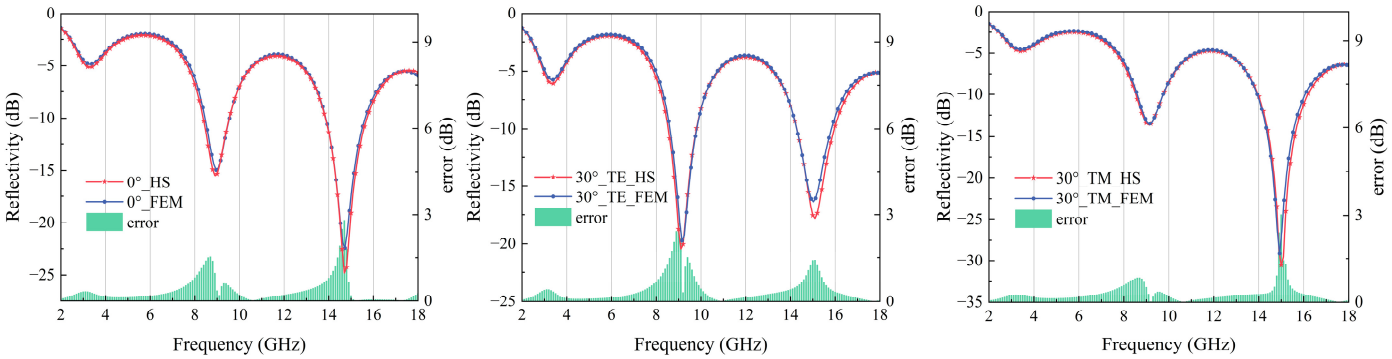

(**a**) 0° incident angle (**b**) 30° incident angle in TE mode (**c**) 30° incident angle in TM mode

Figure 3. Reflectivity comparison of HS and FEM results for different EM incident angles.

We further compare our method with the experimental data presented in Ref. [39], and the results are illustrated in Figure 4. The experimental setup described in Ref. [39] utilized the arched frame test method, and the frequency band ranged from 2 to 18 GHz. The geometric dimensions of the honeycomb test sample were 200 mm × 200 mm × 20 mm. The

honeycomb was structured into three layers along the height, with each layer impregnated with an absorbing coating of varying thickness. Specifically, the coating thickness increased from the top layer to the bottom layer as 12.5 μm, 25 μm, and 37.5 μm respectively. The aperture of the honeycomb was 1.83 mm, and the wall thickness was 0.1 mm.

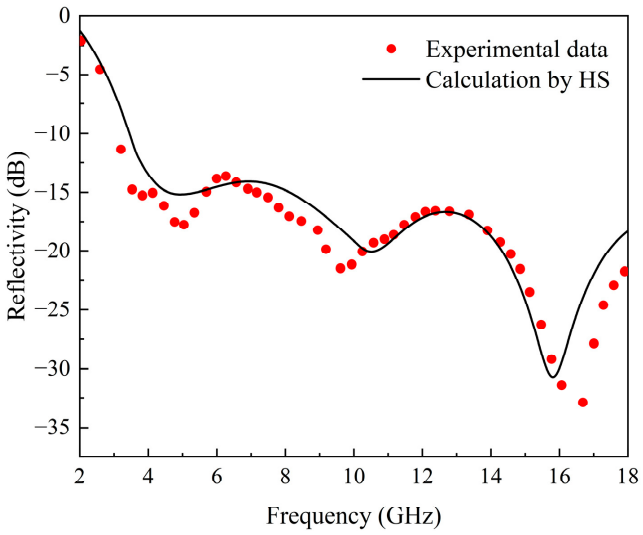

Figure 4. Reflectivity comparison of HS and experimental data in Ref. [39].

The comparison results presented above demonstrate that the methods employed in this study to calculate the electromagnetic properties of an HAS possess high credibility. This establishes a solid foundation for their application in subsequent research.

2.5. Optimization Model

The PSO algorithm offers several advantages, including rapid convergence, minimal parameter requirements, and straightforward implementation. However, it is also susceptible to being trapped in local optima, a phenomenon often referred to as "premature". To enhance the optimization performance of the algorithm and to increase the diversity within the particle population, it is beneficial to employ varied velocity and position update strategies for particles that represent the global optimum. The formulas for updating the velocity and position of these optimal particles in each iteration are as shown below.

$$V_{\tau,j}^{k+1} = -X_{\tau,j}^{k} + p_{gd} + \omega V_{\tau,j}^{k} + \rho(t)(1 - 2r_2(t)) \tag{19}$$

$$X_{\tau,j}^{k+1} = X_{\tau,j}^{k} + V_{\tau,j}^{k+1} = p_{gd} + \omega V_{\tau,j}^{k} + \rho(t)(1 - 2r_2(t)) \tag{20}$$

where τ is the current best particle, p_{gd} is the global optimal position, and $\rho(t)$ is the scaling factor. This can make the best particle randomly search near the global optimal position, specifically defined as

$$\rho(t+1) = \begin{cases} 2\rho(t) & if\ successes > s_c \\ 0.5\rho(t) & if\ failures > f_c \\ \rho(t) & otherwise \end{cases} \tag{21}$$

where *successes* represents the updated global optimal position, and *failures* indicates that the global optimal position has not been updated. s_c and f_c need to be set according to specific functions, generally based on experience; they can be set to s_c = 15 and f_c = 5.

The improved optimization algorithm exhibits significant advantages in terms of convergence when compared with the traditional PSO algorithm. For details on the specific algorithm validation process, refer to the paper [40]. This study employs the improved

PSO algorithm, implemented in C++, to develop the corresponding software. The detailed process of the algorithm is illustrated in Figure 5.

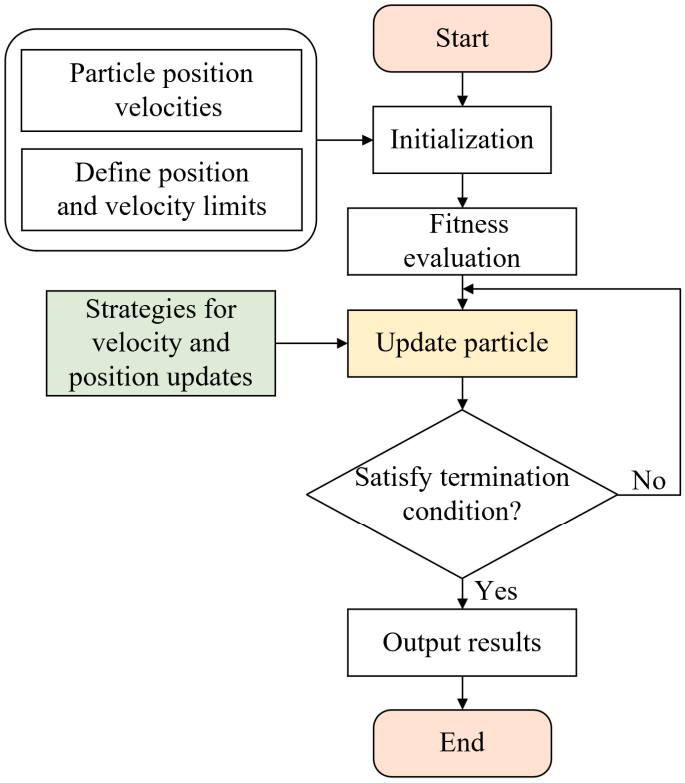

Figure 5. Flowchart of improved PSO algorithm.

When the absorbing structure has a large absorption bandwidth and good angular stability, we believe that the absorbing performance of the structure is better. Based on the requirements for absorption bandwidth and incident angle, we select the maximum number of detection points with reflectivity lower than the target reflectivity R_0 within the incidence frequency and incident angle ranges of interest as the objective function. And the target reflectivity R_0 is set to -10 dB. Specifically, we discretize the absorption frequency and the incident angle and define the number of frequencies is as N_f and the number of incident angles as N_{angle}. Then, a two-dimensional decision matrix M_{ij} is introduced, whose size is $N_f \times N_{angle}$, and the initial values of the elements in the matrix are set to 0. If the reflectivity of an HAS is lower than R_0 at the i-th detection frequency and j-th incident angle, $M_{ij} = 1$; otherwise, $M_{ij} = 0$. While, for the two polarization modes, there are M_{ij}^{TE} and M_{ij}^{TM}, respectively, only when the values of M_{ij}^{TE} and M_{ij}^{TM} are both equal to 1 does the corresponding M_{ij} equal to 1. Therefore, the final form of the objective function is set as in Equation (22).

$$objective = 1 - \sum_{i=1}^{N_f} \sum_{j=1}^{N_{angle}} (M_{ij}^{TE} \times M_{ij}^{TM}) / (N_f \times N_{angle}) \tag{22}$$

As demonstrated by the preceding formulas, the value of the objective function varies from 0 to 1, with lower values indicating superior wave absorption performance of the HAS.

3. Results and Discussion

3.1. Single-Layer Honeycomb Absorbing Structure

Based on the above methods, we optimize the single-layer NHAS and GHAS, and compare the results for both structures. The HAS possesses numerous structural parameters,

offering a substantial optimization space to regulate its absorbing performance. The material parameters of the honeycomb framework, coating medium, and absorbing skin are detailed in Table 1. For the single-layer HAS, RAM1 is selected as the coating medium. In alignment with actual processing and application requirements, the design variables and their value ranges for the HAS are presented in Table 3. The side length r of the honeycomb aperture influences the resonant frequency and reflectivity. We maintain r at a constant value to reduce computational load, as the HS method primarily involves the duty cycle and material parameters of each component, and other dimensional parameters are varied.

Table 3. Design parameters and range of single-layer HAS.

Target	**Honeycomb Framework**			**Coating Medium**		**Skin**
Parameter	r	w	h	d_{top}	d_{bottom}	d_{skin}
Value range (mm)	6	0.5~2	1~10	0.1~2	0.1~2	0.5~2

Table 4 presents the optimization results for the single-layer NHAS and GHAS across the frequency range of 2–18 GHz. The table reveals that after optimization, both the coating and skin thicknesses of the NHAS reach their upper limits of 2 mm, resulting in a final objective function value of 0.83. In contrast, for the GHAS, the honeycomb framework has a thickness of 0.5 mm, and the height reaches the maximum of 10 mm. The coating medium's thickness linearly increases from 0.1 mm at the top to 2 mm at the bottom, corresponding to an objective function value of 0.56. Compared with the NHAS, the absorbing properties of the GHAS are significantly enhanced. This improvement is primarily due to the gradient structure's ability to adjust the thickness of the impregnated material, facilitating impedance matching with free space. Consequently, EM waves can more readily penetrate the structure, maximizing energy absorption.

Table 4. Optimization results of single-layer HAS.

	NHAS	**GHAS**
w	1.39	0.5
h	2.69	10
d_{top}	2	0.1
d_{bottom}	2	2
d_{skin}	2	0.63
Objective function value	0.83	0.56

Figure 6 depicts the reflectivity curves for two types of single-layer HASs. In Figure 6a, the comparison curves clearly show that the reflectivity of the GHAS is lower than that of the NHAS across most frequencies, with values below −10 dB in both the X (8–12 GHz) and Ku (12–18 GHz) bands. The GHAS exhibits three wave absorption peaks at the frequencies of 3 GHz, 8 GHz, and 12.7 GHz, whereas the NHAS displays only two, at 6 GHz and 17 GHz. This difference arises because, in the GHAS, the electromagnetic properties of the materials vary along the principal axial direction. Such variation alters the local wave speed and impedance within the structure, changing the resonant frequencies at different positions. Consequently, specific resonance modes may develop in various areas, potentially overlapping or interfering with each other across the structure. This interaction can lead to the formation of multiple resonance points and, ultimately, a greater number of absorption peaks. In contrast, the properties of the NHAS remain constant along the principal axial direction, resulting in fewer wave absorption peaks compared with the GHAS.

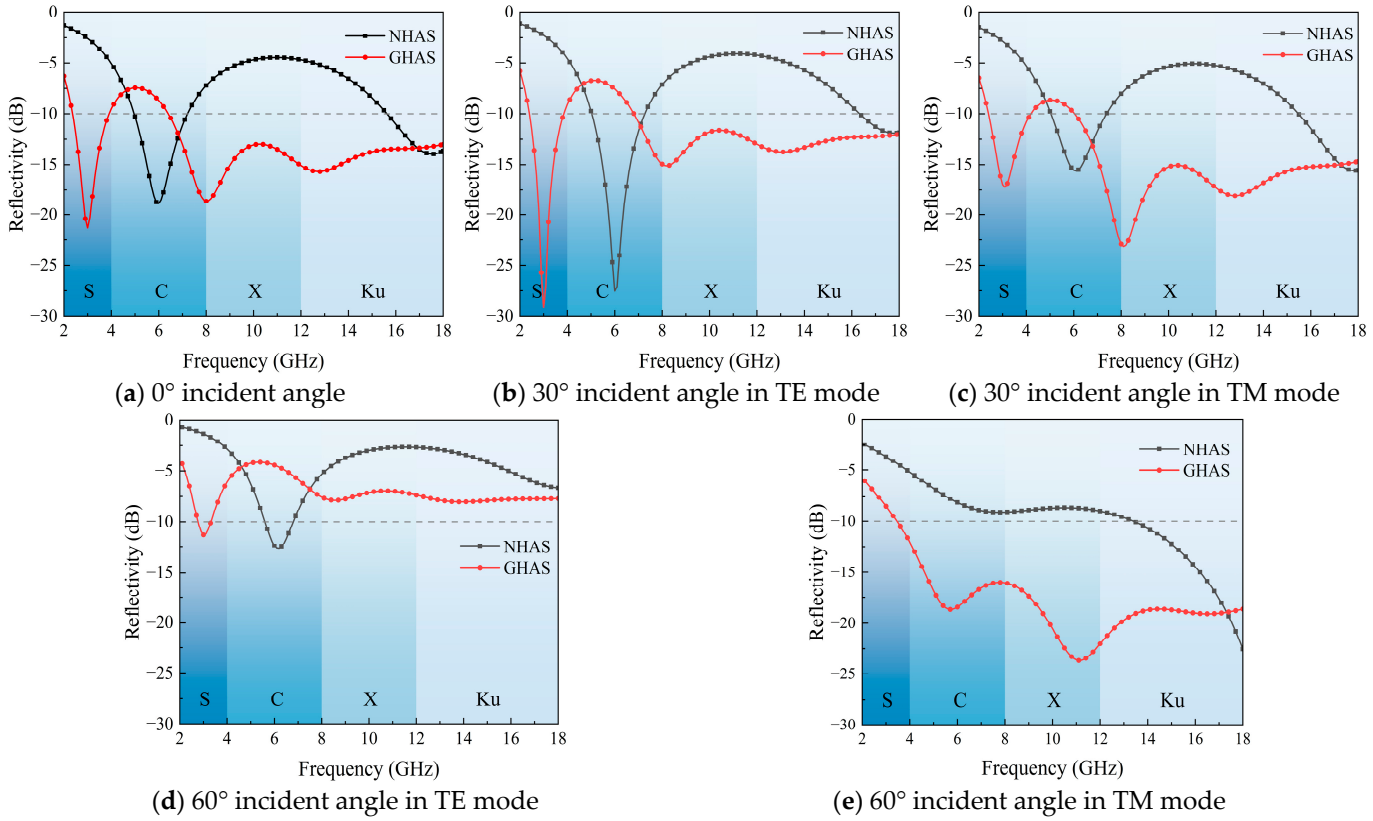

(**a**) 0° incident angle (**b**) 30° incident angle in TE mode (**c**) 30° incident angle in TM mode

(**d**) 60° incident angle in TE mode (**e**) 60° incident angle in TM mode

Figure 6. Reflectivity of NHAS and GHAS at different incident angles in two polarization modes.

The calculated results for a 30° incident angle are shown in Figure 6b,c. Under both polarization modes, the GHAS continues to demonstrate superior absorbing performance. Although the reflectivity exceeds −10 dB at a few frequencies within the low-frequency bands (S (2–4 GHz) and C (4–8 GHz)), it remains below −10 dB across the majority of frequencies. For a larger oblique incident angle of 60°, the results, shown in Figure 6d,e, indicate a significant disparity between the TE and TM polarization modes. In TM polarization mode, the GHAS exhibits enhanced wave absorption capabilities. Table 5 shows the absorption bandwidths of the NHAS and GHAS below −10 dB at different incident angles. The data from the table confirm that the GHAS maintains a broader absorption bandwidth than the NHAS even at large oblique incident angles. Furthermore, the absorption frequency band shifts towards the lower frequency range, suggesting that the GHAS also performs better in absorbing low-frequency waves.

Table 5. Absorption bandwidths of NHAS and GHAS.

	NHAS		**GHAS**	
	−10 dB Bandwidths (GHz)	**Fractional Bandwidths**	**−10 dB Bandwidths (GHz)**	**Fractional Bandwidths**
0°	4.7	36.07% (5–7.2 GHz) 13.65% (15.7–18 GHz)	13.3	47.62% (2.4–3.9 GHz) 95.08% (6.4–18 GHz)
30° TE	3.9	34.15% (5.1–7.2 GHz) 9.3% (16.4–18 GHz)	12.7	45.16% (2.4–3.8 GHz) 89.16% (6.9–18 GHz)
30° TM	4.9	35.48% (5.1–7.3 GHz) 14.93% (15.5–18 GHz)	13.7	48.49% (2.5–4.1 GHz) 98.76% (6.1–18 GHz)
60° TE	1.9	29.03% (5.3–7.1 GHz)	0.6	16.39% (2.8–3.3 GHz)
60° TM	4.6	28.57% (13.5–18 GHz)	14.6	134.88% (3.5–18 GHz)

In order to further analyze the frequency characteristics and angle sensitivity of the GHAS, Figure 7 shows the reflectivity contours of the GHAS in the bandwidth of 2–18 GHz and the incident angle range of 0°~80° under two polarization modes. We find that under TE polarization, the reflectivity at large bandwidth is less than −10 dB within the incident angle range of 0°~60°. Under TM polarization, it exhibits excellent absorption effects over a wider range of angles. This indicates that the GHAS has good angular stability and wider absorbing bandwidth. In addition, it can be observed from the figure that the reflectivity is relatively high within the 4–6 GHz frequency range, which may be related to the geometric design of the honeycomb structure. The ideal absorbing effect can be achieved by adjusting the unit size, thickness, the number of honeycomb layers, and the material properties. Discussion on the impact of the latter two modifications will be detailed in the following section.

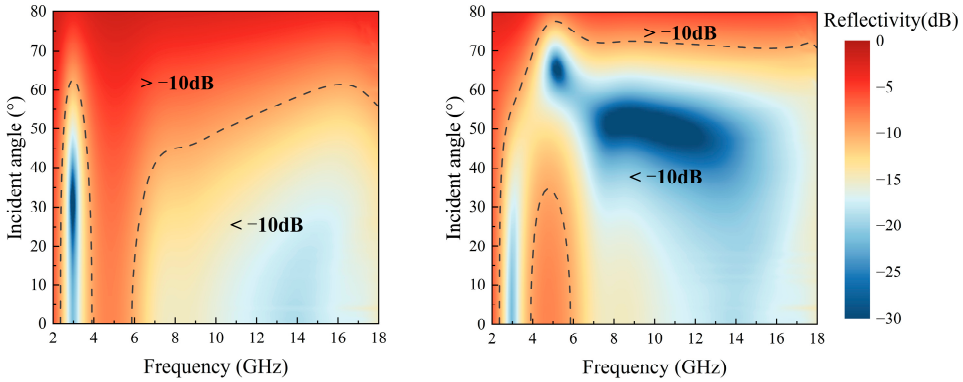

(**a**) TE mode (**b**) TM mode

Figure 7. Reflectivity under oblique incidence waves in two polarization modes.

The absorption mechanism is further explored by analyzing the distribution of electric fields on a specific slice plane. The specific position of the slice plane is shown in Figure 8a. Figure 8b,c show the field distribution contours at on Plane 1. By comparing the electric field of gradients and normal structures at the same phase shown in the figure, the electric field intensity of the GHAS is relatively strong in the upper part and weaker in the lower part. This observation suggests that EM waves are gradually absorbed and lost during propagation, supporting the hypothesis that gradient designs enhance the reduction of in EM wave reflection and improve absorption performance. However, the electric field intensity of the NHAS is still relatively high near the metal substrate, indicating inefficient absorption within the structure due to poor impedance matching. The honeycomb structure displays pronounced symmetry within Plane 2, leading to a relatively uniform electric field intensity in this direction; therefore, further analysis of the electric field intensity on this plane is not required.

Figure 9 depicts the electric field vector diagram for slice Plane 2, illustrating how EM waves experience deflection during propagation across different media. This deflection facilitates an increase in the number of reflections and scattering of EM waves within the absorbing structure, thereby enhancing energy loss. However, the electric field vector on Plane 1 is influenced by the uneven distribution of materials along the GHAS principal axis, which makes it less valuable for reference; analysis of the electric field vector on Plane 1 is unnecessary.

Figure 10 provides the Smith chart for the two absorbing structures, where the blue coverage area denotes the −10 dB absorption range. Compared with the NHAS, a greater number of frequency points on the GHAS curve are located within the blue area. Additionally, the impedance value of the GHAS is closer to (1, 0), suggesting that the optimized GHAS enhances impedance matching between free space and the absorbing structure. This improvement in impedance matching significantly boosts the absorption performance of the HAS.

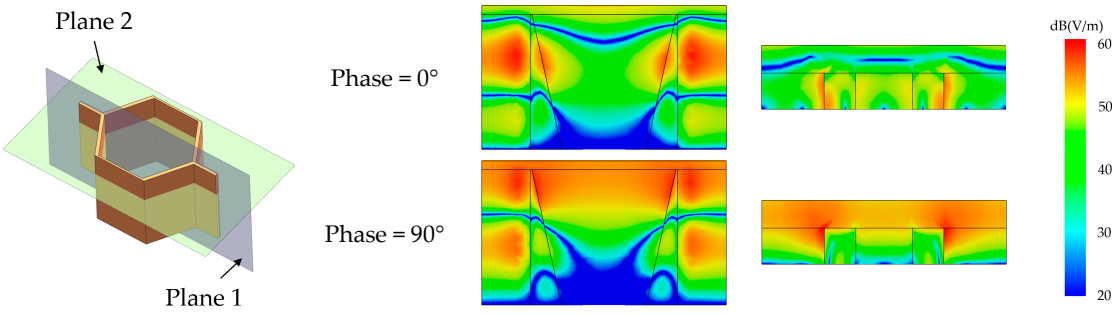

(**a**) The schematic of slice planes (**b**) Electric field distribution in GHAS (**c**) Electric field distribution in NHAS

Figure 8. The schematic of the slice planes and electric field distribution in the GHAS and NHAS at 10 GHz at various phases.

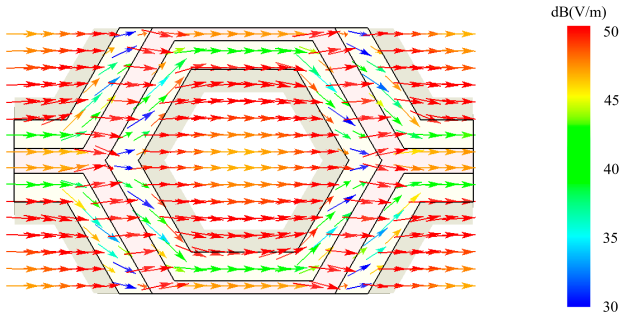

Figure 9. Field vector distribution on slice plane of GHAS.

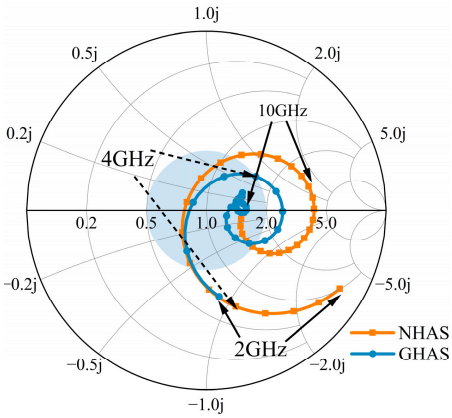

Figure 10. Smith chart comparison of NHAS and GHAS.

Based on the above comparative analysis of the NHAS and GHAS, we find that the GHAS has a wider absorption bandwidth and more absorption peaks, along with improved angular stability, which can absorb and dissipate electromagnetic waves more effectively.

3.2. Optimization of Multi-Layer Gradient Honeycomb Absorbing Structure

Compared with the NHAS, the GHAS has better impedance matching characteristics with free space. To further improve the absorption performance of the GHAS, this paper proposes a multi-layer gradient honeycomb structure (MGHAS). The cross-sectional schematic of the MGHAS, depicted in Figure 11, includes a top skin, honeycomb cores, bonding layers, and a reflective layer. The thickness of each layer of honeycomb core absorbing coating is expressed as d_i^{top} and d_i^{bottom}, where i = 1, 2, 3. Taking into account the limitations of actual processing and application on the number and thickness of honeycombs, we mainly consider the three-layer honeycomb absorbing structure here. The

thickness range is from 0.1 mm to 2 mm. The total height limit for multi-layer absorbing structures is adjusted to the range of 1 to 20 mm. The subsequent analysis primarily investigates the effects of various coating media and sorting methods on the optimization results. The range of design variables remains consistent with that of the single-layer structure, as detailed in Table 3. The optimized structure will subsequently be applied to the aircraft inlet, the details of which will be provided in the following section. Table 6 outlines the different approaches to the coating medium.

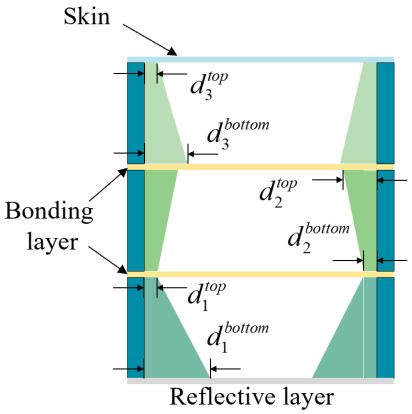

Figure 11. Cross-sectional schematic of proposed MGHAS.

Table 6. Compositions and sequence of coating media.

Samples	1st Layer Material	2nd Layer Material	3rd Layer Material
Case-1	RAM1	RAM1	RAM1
Case-2	RAM2	RAM2	RAM2
Case-3	RAM3	RAM3	RAM3
Case-4	RAM3	RAM1	RAM2
Case-5	RAM2	RAM1	RAM3

As illustrated in Table 6, the schemes in Case-1, Case-2, and Case-3 each utilize a single type of RAM. Typically, the absorbing performance of RAMs is heavily influenced by the material's loss tangents. In contrast, the schemes in Case-4 and Case-5 involve the use of three different materials, sorted by their dielectric loss tangents. Specifically, Case-4 is designed such that the dielectric loss tangents of each layer in the impregnated medium decrease progressively from the reflective layer to the skin. Conversely, Case-5 arranges the materials in the opposite order, where the dielectric loss tangents increase towards the skin.

Table 7 shows the optimization results for the multi-layer GHAS. Initially, the analysis focuses on the schemes in Case-1, Case-2, and Case-3, wherein each of the three-layer honeycomb cores adopts a single type of RAM. In these three schemes, d_3^{top} is minimized to the lower limit of 0.1 mm to enhance impedance matching with free space. Conversely, d_1^{bottom} is maximized to the upper limit of 2 mm, enabling more extensive absorption of the EM waves incident on the absorbing structure. The height difference across the five schemes is relatively small. Among the various schemes, the Case-3 scheme has the smallest objective function value, indicating that it has relatively excellent absorbing performance. This enhanced performance is primarily attributed to the properties of RAM3, which features high dielectric and magnetic loss tangents, thereby facilitating more effective absorption of EM waves. Additionally, the performances of the Case-4 and Case-5 schemes, which utilize different RAMs, are analyzed. Case-4 presents a smaller objective function value, signifying better absorbing performance, primarily due to the small loss tangents of the electromagnetic loss angle of RAM2, located near the honeycomb skin. This layer acts as a wave-transmissive layer, allowing EM waves to penetrate deeper into the structure.

As the EM waves progress into the interior, the electromagnetic loss capability of the honeycomb core intensifies, resulting in progressively better absorption characteristics and continuous loss of EM waves. Conversely, Case-5 does not exhibit the advantages seen in Case-4 because the sequence of RAMs used is reversed, leading to a larger objective function value and inferior wave absorption performance.

Table 7. Optimization results of five different cases.

		Case-1	Case-2	Case-3	Case-4	Case-5
Objective function value		0.43	0.63	0.34	0.32	0.48
h_{total}		19.08	19.37	17.43	19.24	19.04
d	d_1^{top}	2	2	1.31	2	1.08
	d_1^{bottom}	2	2	2	1.88	2
	d_2^{top}	0.78	1.79	0.10	0.12	2
	d_2^{bottom}	2	2	0.50	0.63	1.49
	d_3^{top}	0.1	0.1	0.1	0.1	0.1
	d_3^{bottom}	0.26	2	0.1	0.1	1.14
h	h_1	7.89	9.41	7.30	7.02	1.31
	h_2	2.59	2.72	4.69	8.16	6.73
	h_3	7.61	6.24	4.44	3.06	10

Figure 12 presents the reflectivity curves of the five approaches. The analysis of these curves reveals that Case-3 and Case-4 have similar absorption bandwidths, which explains the close objective function values of these two schemes. Further comparison between the two schemes shows that Case-4 has two strong wave absorption peaks at 4.4 GHz and 10 GHz, while Case-3 has only one wave absorption peak at 5.3 GHz. In addition, near the 10 GHz wave absorption peak, the reflectivity of Case-4 is already lower than −30 dB, indicating an excellent wave absorption effect. Therefore, overall, the Case-4 scheme has the best wave absorption characteristics. By analyzing and comparing the calculation results of different schemes, we find that for the MGHAS, applying an impregnated medium with a smaller dielectric loss tangent to the honeycomb core close to the absorbing skin can improve the impedance matching between the HAS and free space. Conversely, using an impregnated medium with a large dielectric loss tangent to the honeycomb core close to the reflective layer enhances the absorption and loss capabilities of EM waves. Such strategic placement of materials within the MGHAS design optimizes its overall wave-absorbing properties.

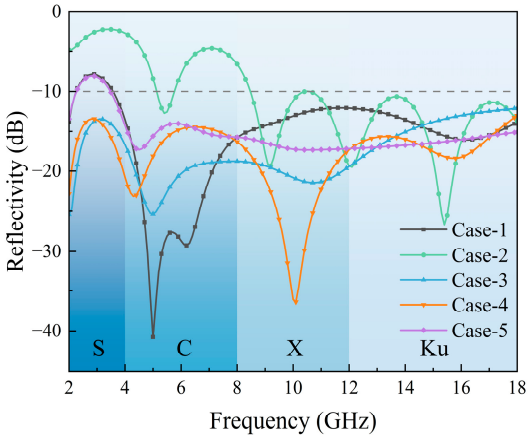

Figure 12. Variations in reflectivity under normal incidence in five different cases.

3.3. Application of Honeycomb Absorbing Structure on Aircraft Inlet

In the optimization design study detailed above, Case-4 emerges as the optimal design scheme for the MGHAS. This section applies Case-4 to the surface of an inlet with oblique angle, analyzes its effectiveness in reducing the RCS value, and contrasts results with those obtained by using traditional coating-type materials. The geometric parameters of the inlet are shown in Table 8 and Figure 13a. The inclined cut angle is $\beta = 60°$, the cross-sectional size of the outlet is 400 mm × 400 mm, and the length of the upper surface of the straight cavity is 1500 mm. We divide the inner surface of the inlet into three area-equal parts, I, II, and III, where part I includes the outlet section of the inlet.

Table 8. Geometric parameters of aircraft inlet.

	L	W	H	β
Parameter	1500 mm	400 mm	400 mm	60°

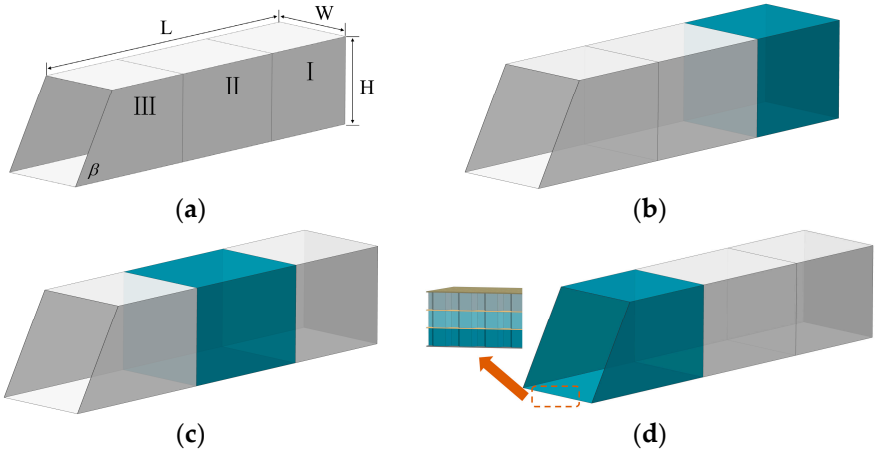

Figure 13. Schematic diagram of geometric parameters and different stealth strategies of inlet: (**a**) model-0; (**b**) model-1 (HAS applied on part I), model-4 (coating-type materials (1 mm) applied on part I), and model-7 (coating-type materials (19.24 mm) applied on part I); (**c**) model-2 (HAS applied on part II), model-5 (coated materials (1 mm) applied on part II), and model-8 (coated materials (19.24 mm) applied on part II); (**d**) model-3 (HAS applied on part III), model-6 (coating-type materials (1 mm) applied on part III), and model-9 (coating-type materials (19.24 mm) applied on part III).

As illustrated in Figure 13, we implemented the HAS and coating-type absorbing materials on the inlet, using model-0, which features an all-metal surface, as a contrast model. The effectiveness of the coating-type material is influenced by its thickness. Based on engineering experience in RAMs on aircraft surfaces, the thickness of the coating material is set to 1 mm [41]. For consistency with the honeycomb structure of Case-4, the height of the absorbing coating material is also designed to be 19.24 mm. It is important to note that such thickness is uncommon for absorbing coatings on aircraft surfaces; this increased thickness is adopted here solely to maintain controlled variables for comparative analysis purposes.

The radar detection angles are set as shown in Figure 14, covering both horizontal and vertical detection planes. The angles range from −60° to 60° with an interval of 1°. Due to the symmetry of the inlet, it is sufficient to consider only the range from 0° to 60° for the horizontal detection plane. In the radar band (S-Ku band) commonly used for aircraft detection, the inlet is classified as an electrically large target. As mentioned earlier, unlike the analysis of the electromagnetic scattering characteristics of electrically large targets coated with general absorbing coatings, the electromagnetic scattering analysis of electrically large targets covered with an HAS faces a contradiction between electrically large size and electrically small size.

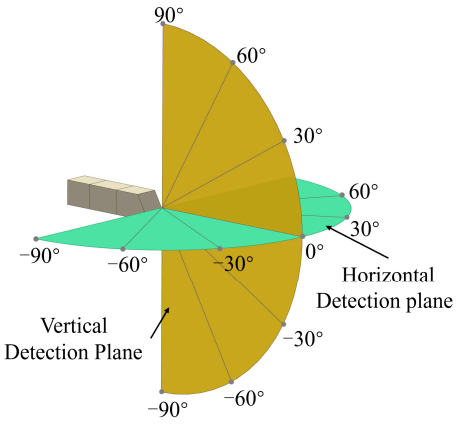

Figure 14. Schematic diagram of detection plane and angle.

The shooting and bouncing ray method (SBR) is one of the effective methods for calculating the electromagnetic scattering of cavity targets and targets with strong surface coupling, which integrates computational efficiency and accuracy. In this paper, referring to the calculation method of EM scattering characteristics of electrically large, coated targets [18,42], reflectivity is introduced into the high-frequency asymptotic method, replacing the reflectivity term in the process of field strength tracking process. This approach resolves the aforementioned contradiction and enables the analysis of the EM scattering characteristics of an aircraft inlet covered with an HAS.

To verify the accuracy of the proposed method, we apply both the FEM and our method to calculate the RCS of a GHAS with a finite size (510 mm × 330 mm). The geometric schematic diagram is shown in Figure 15a, while the calculation results are shown in Figure 15b. Within the range of 0°~30°, the results of the two methods are relatively close, especially in the range of 0°~15°, where the calculation results of the two methods match very well. As the incident angle of EM waves increases, the changing trends remain similar, and the results stay within an acceptable range.

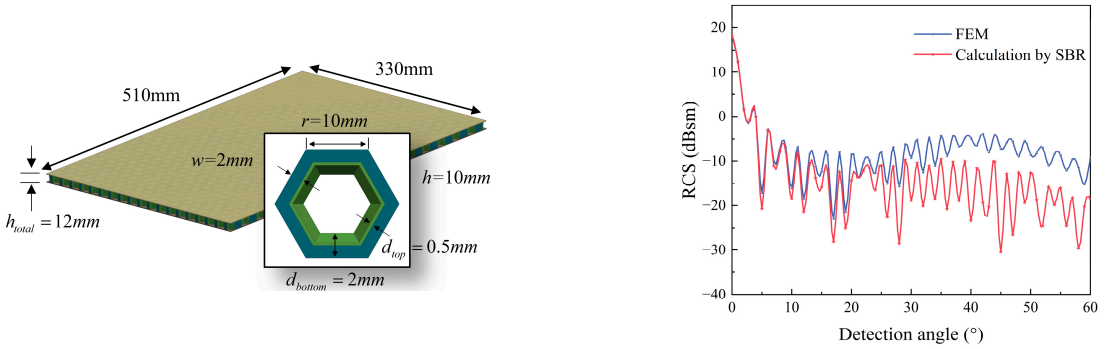

(**a**) Schematic diagram of GHAS plate (**b**) Comparison of FEM and improved SBR method

Figure 15. Schematic diagram of honeycomb plate and comparison results.

The following section elucidates the reasons for the discrepancies between the two computational results. The honeycomb plate is a finite structure; when the incident angle of electromagnetic waves increases, the outermost honeycomb framework is irradiated by EM waves. The FEM accounts for the scattering effects of this part, considering the finite dimensions of the structure. In contrast, when we use the SBR method, the honeycomb structure is equivalent to an infinitely large periodic structure firstly. After obtaining its reflectivity and other parameters, we assign them to a finite plate. This approach does not account for the edge scattering effects of the honeycomb panel, leading to variations in the calculation results between the two methods. However, it can be foreseen that as the size of the honeycomb plate structure increases, the discrepancies between the two methods will

gradually decrease, but this means more computing resources. To reflect the advantages of using the SBR method, we record the resources required to calculate the RCS of the finite-sized honeycomb plate in Figure 15a by using both methods. The results are shown in Table 9. According to the data in the table, the number of meshes divided by the FEM is approximately 471 times and the time consumed is about 933 times longer than that required by the SBR method. Therefore, for the purposes of this study, the SBR method can quickly obtain results within an acceptable range of computational accuracy.

Table 9. Comparison of FEM and SBR calculation resources and duration.

	Number of Cores	Number of Meshes	Required Time
FEM	12	1.81 million	23.58 h
SBR	12	3844	91 s

We use SBR to simulate the EM scattering characteristics of the inlet covered with the HAS and coated with the RAM. Subsequently, we analyze and compare their effects on inlet RCS reduction. Figure 16a,b provide the RCS distribution curves for different schemes for a horizontal plane and two polarization modes respectively. In these figures, the green areas with vertical stripes indicate that the RCS value for the HAS scheme is lower than that for coated RAM scheme, while the orange areas with horizontal stripes show the opposite.

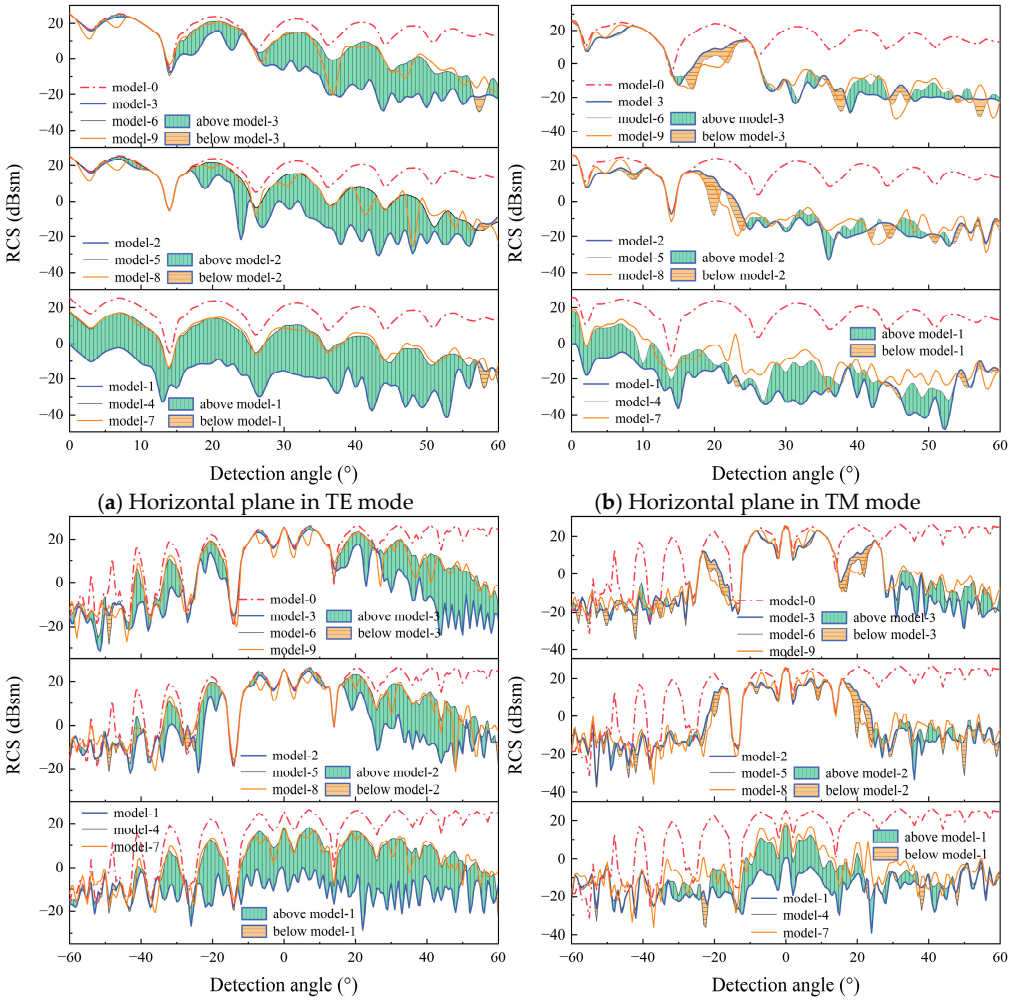

(**a**) Horizontal plane in TE mode (**b**) Horizontal plane in TM mode

(**c**) Vertical plane in TE mode (**d**) Vertical plane in TM mode

Figure 16. RCS angular distribution curves on two detection planes in different modes.

As the detection angle increases, the RCS values of different schemes fluctuate and decrease. The curves show that regardless of the polarization mode, the application of both HAS and RAM coatings can significantly reduce the RCS of the inlet, with the HAS proving more effective, particularly for model-1. For instance, at a 0° forward detection angle, the RCS values are 25.53 dBsm (TE) and 25.59 dBsm (TM) for model-0. The corresponding values of model-1 are just −0.60 dBsm (TE) and −0.32 dBsm (TM), marking a significant reduction from model-0. On the other hand, model-4 shows RCS values of 17.51 dBsm (TE) and 17.64 dBsm (TM), and model-7 records 18.35 dBsm (TE) and 18.10 dBsm (TM). The coating-type material schemes with the same thickness as the HAS do not further enhance the absorption characteristics. By comparison, using an HAS at the same location has a more significant effect. This phenomenon can be attributed to the application of an HAS on the outlet end face of the inlet. At a detection angle of 0°, electromagnetic waves can directly illuminate the HAS surface, resulting in significant absorption. As the HAS is an anisotropic structure, it can be seen from its reflectivity that its absorbing ability decreases when the angle between the incident direction of EM waves and the principal axis of the HAS increases. For model-2 and model-3, when the incident angle is small, the angle between the incident direction of the electromagnetic wave and the principal axis of the HAS is relatively large. Simultaneously, the EM wave directly irradiates the outlet end face of the inlet, resulting in specular reflection and consequently strong echoes. As a result, these two schemes demonstrate inferior RCS reduction effects on the inlet compared with model-1.

Figure 16c,d illustrate the RCS curves in the vertical plane for different configurations under two polarization modes. Models 1 to 9 demonstrate altered RCS distribution curves compared with model-0, particularly for detection angles ranging from 0° to 60°. This pattern is similar to that observed on the horizontal plane. Notably, model-1 consistently exhibits superior RCS reduction effects across both polarization modes, with a more pronounced reduction observed in TE mode.

Figure 17 shows the mean RCS of different schemes. To clearly differentiate between these schemes, the mean RCS values are divided into two parts by 0 dBsm. Among them, the mean RCS values for model-1 are below 0 dBsm, while the RCS values of other schemes exceed 0 dBsm. Compared with model-0, all nine schemes using the HAS or coating-type material demonstrate a reduction in the mean RCS to varying extents. model-1 exhibits the best RCS reduction effect, followed by model-4, consistent with findings in Figure 16. On the horizontal plane, the mean RCS values of model-1 are only −12.79 dBsm (TM) and −11.05 dBsm (TE). These results affirm that the HAS offers a superior absorption capability compared with traditional absorbing coating-type materials. The effectiveness of the HAS is notably enhanced when applied to the surface of the inlet, significantly affecting the electromagnetic scattering properties of the inlet. Moreover, it is crucial to minimize the angle between the electromagnetic wave and the principal axis of the HAS to maximize its absorbing efficiency.

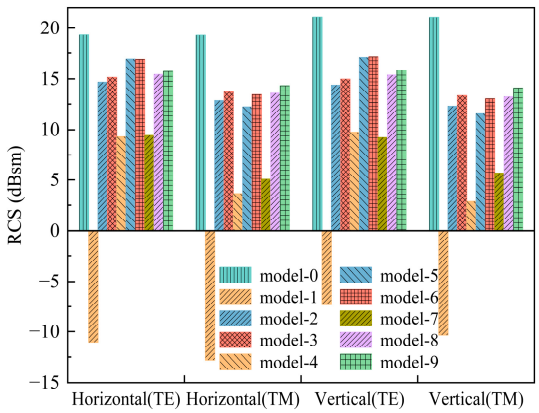

Figure 17. Mean RCS with different approaches on two detection planes.

4. Conclusions

In this paper, the homogenization method is applied to evaluate the EM absorption performance of an NHAS and a GHAS, and the mechanism of gradient design is studied. Then, an MGHAS with top skin and bonding layers is proposed, and the influence of the material type and arrangement on reflectivity is analyzed. An improved PSO algorithm is applied to optimize the EM absorption performance of the MGHAS. The results demonstrate that the optimized MGHAS achieves a reflectivity below −10 dB across the 2–18 GHz frequency range. Finally, reflectivity is introduced into the shooting and bouncing ray method to solve the problem of periodic structures applied to electrically large targets. This enhanced method is then employed to investigate the electromagnetic scattering characteristics of aircraft inlet equipped with an MGHAS. The results suggest that the proposed MGHAS can significantly reduce the RCS of the aircraft inlet compared with those without stealth technologies and those with coating-type absorbing materials. The main work and conclusions are summarized as follows:

(1) The homogenization method is applied to study the EM wave absorption characteristics of an NHAS and a GHAS at various bandwidths and angles. The impact patterns and mechanisms of gradient design in impregnation materials are analyzed. An MGHAS is proposed; it primarily comprises a top skin, middle honeycomb cores, bonding layers, and a bottom reflective layer. The impact of the selection and sequence of impregnated materials within the honeycomb core is investigated. Research has demonstrated that using an impregnated material with a smaller electromagnetic loss tangent near the top skin allows this layer to act as a transmission medium, thereby enhancing the impedance matching between the honeycomb absorber structure and free space. Incorporating an impregnated material with a higher dielectric loss tangent near the bottom reflective layer significantly enhances the dissipation of electromagnetic waves, thereby maximizing EM wave absorption. An improved PSO algorithm is employed to optimize the electromagnetic absorption performance of the MGHAS. The results indicate that the reflectivity of the optimized MGHAS is below −10 dB in the frequency range of 2–18 GHz, demonstrating that the proposed MGHAS structure exhibits effective electromagnetic wave absorption properties.

(2) Both the application of the MGHAS and the coating-type absorbing materials reduce the RCS of the aircraft inlet. However, the RCS reduction achieved with the MGHAS is more substantial than that achieved with the coating-type absorbing material. The scheme of applying an MGHAS to the inlet end face and adjacent surface reduces the RCS of the inlet at the 0° detection angle and 10 GHz frequency, achieving reductions of 99.74% (TM; horizontal plane) and 99.76% (TE; vertical plane) compared with an inlet without stealth technologies. The mean RCS of the inlet equipped with the MGHAS approaches −20 dBsm. In contrast, the mean RCS of the inlet without stealth technologies is approximately 10 dBsm, and the mean RCS of the inlet with the coating-type material also exceeds −10 dBsm. Furthermore, due to the anisotropic properties of the honeycomb absorber structure, the optimal placement of the structure is closely related to the angle of incidence of the EM waves. It is advisable to align the principal axis of the honeycomb structure as closely as possible with the direction of the incident waves.

(3) Given that HASs typically need to withstand mechanical loads when applied to aircraft, it is essential to comprehensively consider both their electromagnetic absorbing and mechanical properties. This comprehensive analysis will be the focus of our subsequent research work.

Author Contributions: Conceptualization, H.X.; methodology, H.X. and Y.H.; software, H.X.; validation, H.X. and Y.H.; formal analysis, H.X.; investigation, H.X., Y.S. and X.W.; resources, Q.Y.; data curation, H.X.; writing—original draft preparation, H.X.; writing—review and editing, H.X. and X.W.; visualization, H.X. and X.W.; supervision, Q.Y.; project administration, Y.S and Q.Y.; funding acquisition, Y.S. All authors have read and agreed to the published version of the manuscript.

Funding: This research was funded by Natural Science Basic Research Program of Shaanxi (grant number 2022JQ-052).

Data Availability Statement: Data are contained within the article.

Conflicts of Interest: Author Yubo He was employed by the company Aerospace Era Feihong Technology Limited Company. The remaining authors declare that the research was conducted in the absence of any commercial or financial relationships that could be construed as a potential conflict of interest.

References

1. Sang, J.H. *Low-Observable Technologies of Aircraft*, 1st ed.; Aviation Industry Press: Beijing, China, 2013; pp. 8–10, ISBN 978-7-5165-0135-1.
2. Ruiz-Perez, F.; López-Estrada, S.M.; Tolentino-Hernández, R.V.; Caballero-Briones, F. Carbon-based radar absorbing materials: A critical review. *J. Sci. Adv. Mater. Devices* **2022**, *7*, 100454. [CrossRef]
3. Fante, R.L.; McCormack, M.T. Reflection properties of the Salisbury screen. *IEEE Trans. Antennas Propag.* **1988**, *36*, 1443–1454. [CrossRef]
4. Watts, C.M.; Liu, X.; Padilla, W.J. Metamaterial Electromagnetic Wave Absorbers. *Adv. Mater.* **2012**, *24*, 98–120. [CrossRef] [PubMed]
5. Fan, H.L.; Meng, F.H.; Yang, W. Mechanical Behaviors and Bending Effects of Carbon Fiber Reinforced Lattice Materials. *Arch. Appl. Mech.* **2006**, *75*, 635–647. [CrossRef]
6. Fan, H.L.; Yang, W.; Chao, Z.M. Microwave absorbing composite lattice grids. *Compos. Sci. Technol.* **2007**, *67*, 3472–3479. [CrossRef]
7. Li, W.; Xu, L.; Zhang, X.; Gong, Y.; Ying, Y.; Yu, J.; Zheng, J.W.; Qiao, L.; Che, S.L. Investigating the effect of honeycomb structure composite on microwave absorption properties. *Compos. Commun.* **2020**, *19*, 182–188. [CrossRef]
8. Baimova, J.A.; Shcherbinin, S.A. Strength and Deformation Behavior of Graphene Aerogel of Different Morphologies. *Materials* **2023**, *16*, 7388. [CrossRef]
9. Laur, V.; Maalouf, A.; Chevalier, A.; Comblet, F. Three-Dimensional Printing of Honeycomb Microwave Absorbers: Feasibility and Innovative Multiscale Topologies. *IEEE Trans. Electromagn. Compat.* **2021**, *63*, 390–397. [CrossRef]
10. Smith, F.C.; Scarpa, F.; Chambers, B. The electromagnetic properties of re-entrant dielectric honeycombs. *IEEE Microw. Guid. Wave Lett.* **2000**, *10*, 451–453.
11. Gao, Z.P.; Luo, Q. Reflection Characteristic of Impregnated Absorbent Honeycomb under Normal Incidence of Plane Wave. *J. Univ. Electron. Sci. Technol. China* **2023**, *32*, 389–394.
12. Wu, L.; Wang, Q.; Tang, Z. Absorbing properties of three dimensional honeycomb-structured absorbing materials. In Proceedings of the 2012 6th Asia-Pacific Conference on Environmental Electromagnetics, Shanghai, China, 6–9 November 2012.
13. Ghosh, S.; Lim, S. Perforated Lightweight Broadband Metamaterial Absorber Based on 3-D Printed Honeycomb. *Antennas Wirel. Propag. Lett.* **2018**, *17*, 2379–2383. [CrossRef]
14. Mei, C.C.; Auriault, J.L.; Ng, C.O. Some Applications of the Homogenization Theory. *Adv. Appl. Mech.* **1996**, *32*, 277–348.
15. Johansson, M.; Holloway, C.L.; Kuester, E.F. Effective electromagnetic properties of honeycomb composites, and hollow-pyramidal and alternating-wedge absorbers. *IEEE Trans. Antennas Propag.* **2005**, *53*, 728–736. [CrossRef]
16. Ouchetto, O.; Jai-Andaloussi, S.; Sekkaki, A.; Zaamoun, S. Analytical Effective Parameters of Artificial Structures. In Proceedings of the 19th International Radar Symposium, Bonn, Germany, 20–22 June 2018.
17. Chen, H.; Shen, R.; Han, L.; Zhou, Y.; Li, F.X.; Lu, H.P.; Weng, X.L.; Xie, J.L.; Li, X.Q.; Deng, L.J. Closed-form representation for equivalent electromagnetic parameters of biaxial anisotropic honeycomb absorbing materials. *Mater. Res. Express* **2019**, *6*, 085804. [CrossRef]
18. Zhao, Y.C. Study on the Extraction Theory and Applications of Equivalent Electromagnetic Parameters of Radar Absorbing Structure. Ph.D. Thesis, Northwestern Polytechnical University, Xi'an, China, 2014.
19. Choy, T.C. *Effective Medium Theory: Principles and Applications*, 2nd ed.; Oxford University Press: Oxford, UK, 2015; pp. 25–28, ISBN 978-0-19-870509-3.
20. Zhu, H.; Gao, J.; Zhao, J.; Wang, T.T.; Feng, X.G.; Liang, F.C.; Wang, Y.S.; Chen, X. Effective medium theory applied to frequency selective surfaces on periodic substrates. *Chin. Opt. Lett.* **2010**, *8*, 1175–1177. [CrossRef]
21. Stogryn, A. The bilocal approximation for the electric field in strong fluctuation theory. *IEEE Trans. Antennas Propag.* **1983**, *31*, 985–986. [CrossRef]
22. Stogryn, A. Strong fluctuation theory equations for electric field second moments in anisotropic media. *IEEE Trans. Antennas Propag.* **1990**, *38*, 1099–1101. [CrossRef]
23. Tsang, L.; Kong, J.A. Scattering of electromagnetic waves from random media with strong permittivity fluctuations. *Radio Sci.* **1981**, *16*, 303–320. [CrossRef]
24. He, Y.F.; Gong, R.Z.; Wang, X.; Zhao, Q. Study on Equivalent Electromagnetic Parameters and Absorbing properties of honeycomb-structured absorbing materials. *Acta. Phys. Sin.* **2008**, *57*, 5261–5266.
25. Zhao, P.; Xu, Y.G.; Wei, F.M.; Liu, T.; Su, D.L. Electromagnetic property of a novel gradient honeycomb composite fabricated by 3D forming. *J. Magn. Magn. Mater.* **2020**, *493*, 165742.

26. Zhou, P.H.; Huang, L.R.; Xie, J.L.; Liang, D.F.; Lu, H.P.; Deng, L.J. Prediction of Microwave Absorption Behavior of Grading Honeycomb Composites Based on Effective Permittivity Formulas. *IEEE Trans. Antennas Propag.* **2015**, *63*, 3496–3501. [CrossRef]
27. Zhao, Y.C.; Ren, F.; He, L.; Zhang, J.S.; Yuan, Y.N.; Xi, X.L. Design of graded honeycomb radar absorbing structure with wide-band and wide-angle properties. *Int. J. Microw. Wirel. Technol.* **2019**, *11*, 143–150. [CrossRef]
28. Khurram, A.A.; Ali, N.; Rakha, S.A.; Zhou, P.H.; Munir, A. Optimization of the carbon coating of honeycomb cores for broadband microwave absorption. *IEEE Trans. Electromagn. Compat.* **2014**, *56*, 1061–1066. [CrossRef]
29. He, F.; Zhao, Y.; Si, K.X.; Zha, D.C.; Li, R.; Dong, J.X.; Bie, S.W.; Jiang, J.J. Multisection step-impedance modeling and analysis of broadband microwave honeycomb absorbing structures. *J. Phys. D Appl. Phys.* **2020**, *54*, 015501. [CrossRef]
30. Choi, J.H.; Jang, M.S.; Jang, W.H.; Kim, C.G. Investigation on microwave absorption characteristics of conductive-coated honeycomb absorber. *Compos. Struct.* **2020**, *242*, 112129. [CrossRef]
31. Shen, R.B. Modeling and Application Research of Electromagnetic Parameters of Honeycomb Absorbing Structure. Master's Thesis, University of Electronic Science and Technology of China, Chengdu, China, 2020.
32. Li, B.; Zhang, F.; Jin, P. Multi-objective optimization of composites sandwich containing multi-layer honeycomb considering load-bearing capacities and EM absorbing characteristics. *Mech. Adv. Mater. Struct.* **2023**, *31*, 4246–4253. [CrossRef]
33. Sun, P.C.; Wang, L.M.; Wang, T.; Huang, J.; Shao, S.W.; Chen, W. Structural Optimization of the Design of a Double-layer Absorbing Honeycomb Composite. *J. Beijing Univ. Chem. Technol. (Nat. Sci. Ed.)* **2019**, *46*, 58–64.
34. Zhang, X.H.; Sun, Q.; Xu, S.F. Optimal Design of Multi-Layer Absorbent Honeycomb Cellular Composite Material Structure. *Key Eng. Mater.* **2017**, *723*, 335–343.
35. Yakovenko, O.; Matzui, L.; Danylova, G.; Zadorozhnii, V.; Vovchenko, L.; Perets, Y.; Lazarenko, O. Electrical Properties of Composite Materials with Electric Field-Assisted Alignment of Nanocarbon Fillers. *Nanoscale Res. Lett.* **2017**, *12*, 471. [CrossRef]
36. Yakovenko, O.S.; Matzui, L.Y.; Vovchenko, L.L.; Oliynyk, V.V.; Zagorodnii, V.V.; Trukhanov, S.V.; Trukhanov, A.V. Electromagnetic Properties of Carbon Nanotube/BaFe12−xGaxO19/Epoxy Composites with Random and Oriented Filler Distributions. *Nanomaterials* **2021**, *11*, 2873. [CrossRef]
37. Hashin, Z.; Shtrikman, S. A Variational Approach to the Theory of the Effective Magnetic Permeability of Multiphase Materials. *J. Appl. Phys.* **1962**, *33*, 3125–3131. [CrossRef]
38. Zhao, Z.S.; Wu, M.Z.; He, H.H. The Reflection of Obliquely Incident Electromagnetic Wave to Radar Absorbing Material. *J. Huazhong Univ. Sci. Technol.* **1998**, *26*, 36–38.
39. Chen, H.Y.; Shen, R.B.; Li, F.X.; He, Q.T.; Li, G.Y.; Lu, H.P.; Weng, X.L.; Xie, J.L.; Zhang, G.R.; Deng, L.J. Equivalent electromagnetic parameters extraction method for graded honeycomb absorbing materials. *Appl. Phys. B Lasers Opt.* **2021**, *127*, 84. [CrossRef]
40. He, Y.B.; Yang, Q.Z.; Gao, X. Comprehensive optimization design of aerodynamic and electromagnetic scattering characteristics of serpentine nozzle. *Chin. J. Aeronaut.* **2021**, *34*, 118–128. [CrossRef]
41. Ananth, P.B.; Abhiram, N.; Krishna, K.H.; Nisha, M.S. Synthesis of radar absorption material for stealth application. *Mater. Today Proc.* **2021**, *47*, 4872–4878. [CrossRef]
42. Yao, J.J. Evaluation of Scattering from Electrically Large and Complex PEC Target Coated with Anisotropic Material and Its Software Realization. Ph.D. Thesis, Wuhan University, Wuhan, China, 2013.

Disclaimer/Publisher's Note: The statements, opinions and data contained in all publications are solely those of the individual author(s) and contributor(s) and not of MDPI and/or the editor(s). MDPI and/or the editor(s) disclaim responsibility for any injury to people or property resulting from any ideas, methods, instructions or products referred to in the content.